DOI: 10.1021/cg100429b

CRYSTAL GROWTH & DESIGN Article

2010, Vol. 10
3522–3530

The Czochralski Growth of $(Lu_{1-x}Gd_x)_2SiO_5$:Dy Single Crystals: Structural, Optical, and Dielectric Characterization

Grażyna Dominiak-Dzik,*,† Witold Ryba-Romanowski,† Radosław Lisiecki,† Piotr Solarz,† Bogusław Macalik,† Marek Berkowski,‡ Michał Głowacki,‡ and Viktor Domukhovski‡

†*Institute of Low Temperature and Structure Research, Polish Academy of Sciences, ul. Okólna 2, 50-950 Wrocław, Poland, and* ‡*Institute of Physics, Polish Academy of Sciences, Al. Lotników 32/46, 02-668 Warsaw, Poland*

Received March 31, 2010; Revised Manuscript Received June 16, 2010

ABSTRACT: The Czochralski growth of Dy^{3+}-doped $(Lu_{1-x}Gd_x)_2SiO_5$ solid solution single crystals with different mixtures of Lu_2SiO_5 and Gd_2SiO_5 oxides ($x = 0$, 0.2, 0.4, 0.6, 0.8, and 1) is reported. It was found that the $(Lu_{1-x}Gd_x)_2SiO_5$ crystals retain structural, physical, and optical properties of Lu_2SiO_5 even for $x = 0.8$. Optical investigation of Dy:$(Lu_{1-x}Gd_x)_2SiO_5$ revealed that the structural disorder of the host brings about a strong inhomogeneous broadening of Dy^{3+} spectral bands while influencing weakly rates of its radiative and nonradiative transitions. Dielectric characteristics of solid solution crystals are presented and discussed. Finally, $(Lu_{1-x}Gd_x)_2SiO_5$ solid solution crystals seem to be an attractive alternative to a Lu_2SiO_5 host for the design of novel phosphors, radiation converters, and lasers owing to a significantly lower melting temperature and hence easier and less expensive manufacturing.

1. Introduction

Binary rare-earth silicate $Re_2O_3-SiO_2$ systems with 1:1 composition create a group of oxyorthosilicates $Re_2(SiO_4)O$ belonging to two different types of monoclinic structures that are determined by a radius of rare earth ion.[1] Representatives of both crystal types are Gd_2SiO_5 (GSO) with the $P2/c_1$ space group (SG No. 14, $Z = 4$) and Lu_2SiO_5 (LSO) described by the $C2/c_1$ one (SG No. 15, $Z = 8$). Both structures contain two groups of anions: isolated $(SiO_4)^{-4}$ ion complexes and non-silicon bonded oxygen ions (denoted as O5) both sharing in the creation of Re^{3+}-cation polyhedra. Each of the structures possesses two nonequivalent cationic sites differing in the point symmetry, coordination number CN, the $Re^{3+}-O^{2-}$ bond lengths, and the number of silicon-bonded (O1−O4) and non-silicon-bonded (O5) oxygen ions in the first coordination sphere of Gd^{3+} and Lu^{3+} ions.

The crystals are of great interest owing to unique thermal and optical properties. Co-doped with Ce^{3+} offer applications as scintillation detectors for positron emission tomography (PET) and new efficient phosphors.[2,3] Both crystals possess a great ability to accommodate rare earth ions, thereby they emerge also as valuable materials for designing new laser systems. Efficient laser action at around 1 μm was reported for the Yb:Lu_2SiO_5 crystal; more than 7 W of laser radiation was obtained under 14.4 W of the incident pump power at 978 nm.[4] It seems that the LSO and GSO crystals doped with Dy^{3+} or Sm^{3+} ions can be promising systems for applications as white-light emitters owing to an intense luminescence in the blue and yellow spectral range. However, a serious disadvantage of the LSO crystal as a host for rare-earth dopants is its high melting point of 2050 °C that is very close to the breakdown temperature of iridium crucible. For a comparison, the GSO crystal melts at 1770 °C. Thus, the growing of $(Lu_{1-x}Gd_x)_2SiO_5$ (LGSO) mixed crystals seems to be an interesting alternative.

In this work, we report the results of investigation of Dy^{3+}-doped $(Lu_{1-x}Gd_x)_2SiO_5$ (LGSO:Dy) mixed crystals grown by the Czochralski technique. The structural, optical, kinetic, and dielectric properties of LGSO:Dy were examined at low and room temperature and discussed with the reference to those of GSO:Dy and LSO:Dy reported in our previous papers.[5,6]

2. Crystal Growth

Single crystals of $(Gd_{1-y}Dy_y)_2SiO_5$ (GSO:Dy) and $(Lu_{1-y}Dy_y)_2SiO_5$ (LSO:Dy) with $y = 0.05$ and solid solution single crystals of $(Lu_{1-x-y}Gd_xDy_y)_2SiO_5$ (LGSO:Dy) with nominal values of $x = 0.192$, 0.384, 0.576, 0.768 and $y = 0.04$ were grown by the Czochralski method in an inductively heated iridium crucible under the nitrogen atmosphere. The starting materials of 99.99% purity were used. They were fired at 1000 °C for 4 h before weighing and mixing. Stoichiometric mixtures of Gd_2O_3 and/or Lu_2O_3 and SiO_2 powders, in a molar ratio of 1:1, were used as starting materials. The admixture of Dy_2O_3 was doped into the mixtures in the place of Lu_2O_3 (LSO, LGSO) and Gd_2O_3 (GSO). Starting materials were mixed together and then pressed into cylinder tablets under a high pressure. The tablets were sintered in a furnace at a temperature of 1500 °C for 6 h before they were loaded into a crucible. Single crystals were grown with a convex crystal melt interface on an iridium 2 mm rod with a pulling rate of 1.5−2 mm/h and a speed of rotation of 20 rpm. Transparent and almost colorless crystals with 20 mm of the diameter were grown from the 40 mm crucible. The plates with orientation (100) and (010) were cut from the crystal boules (Figure 1) and used in our experiments. A strong tendency to cracking parallel to the cleavage plane (100) was observed for the GSO:Dy sample. The composition analysis of the solid solution crystals was carried out with an inductively coupled plasma (ICP)

*Corresponding author: Tel.: (48-71) 343 50 21. Fax: (48-71) 344 10 29. E-mail: G.Dominiak-Dzik@int.pan.wroc.pl.

 Published on Web 07/09/2010

instrument. The results are gathered in Table 1 together with the nominal compositions and the sample denotations used in the paper.

3. Experimental Techniques

The structure of the crystals was investigated at room temperature by means of the precise powder X-ray diffraction method using a Siemens D5000 diffractometer with filtered CuKα radiation and scintillation counter as a detector. The diffraction patterns were measured with a step of 0.02° and an averaging time of 10 s/step. The experimental data were analyzed by the Rietveld refinement method using the R.A. Young DBWS-9807 package[7] that enabled us to take into account positional and thermal corrections, scaling factor, zero shift, background parameter, Bragg-peak profile parameter, and extinction correction. Density of the samples was determined by both the X-ray and immersion methods. Unpolarized optical measurements were carried out at 12 and 300 K. Absorption spectra were recorded with a Varian 5E UV−vis-NIR spectrophotometer. The vacuum-ultraviolet VUV measurements (excitation and emission spectra) were carried out under synchrotron radiation at the SUPERLUMI station of Hamburger Synchrotronstrahlungslabor (HASYLAB) at Deutsches Elektronen-Synchrotron (DESY). The excitation spectra were corrected for the incident flux of the excitation beam using the sodium salicylates as a standard. The low-resolution emission spectra, obtained under the VUV excitation, were recorded with a CCD camera. The high-resolution luminescence measurements were carried out using an Optron Dong Woo Fluorometer System containing ozone-free Xe lamp as an excitation source. Kinetics experiments were carried out with a Surelite Optical Parametric oscillator (OPO) pumped by a third harmonic of a Nd:YAG. The emitted light was detected by a photomultiplier connected to a Tektronix TDS 3052 oscilloscope. A continuous flow liquid helium cryostat Oxford model CF 1204 equipped with a temperature controller was used to low-temperature measurements carried out in our laboratory. Dielectric properties were measured in the 5×10^{-1} to 10^5 Hz frequency range by a Novocontrol GmbH Alpha Analyzer equipped with a NorECs SA heating system and high temperature sample holder with solid platinum electrodes. The measurements were performed in the 300−1070 K temperature range with a step of 20 K, under the normal pressure and at a flow of dry air atmosphere. The stabilization of temperature was ±0.5 K. Samples in the form of plates with the (010) orientation and dimension of 9 × 4.7 × 1.2 mm were used.

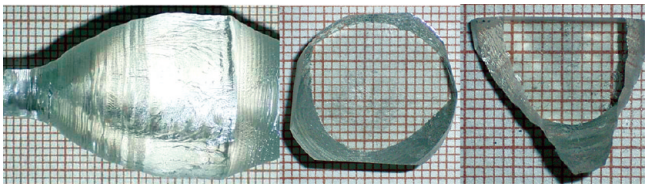

Figure 1. Photographs of the $(Lu_{1-x}Gd_x)_2SiO_5$:Dy solid solution crystal.

Table 1. Nominal and Real Compositions of Dysprosium-Doped Oxyorthosilicate Single Crystals

composition of $(Lu_{1-x-y}Gd_xDy_y)_2SiO_5$		
melt	crystal	denotation
$(Lu_{0.95}Dy_{0.05})_2SiO_5$		LSO
$(Lu_{0.768}Gd_{0.192}Dy_{0.04})_2SiO_5$	$(Lu_{0.799}Gd_{0.163}Dy_{0.038})_2SiO_5$	80Lu-20Gd
$(Lu_{0.576}Gd_{0.384}Dy_{0.04})_2SiO_5$	$(Lu_{0.634}Gd_{0.331}Dy_{0.035})_2SiO_5$	60Lu-40Gd
$(Lu_{0.384}Gd_{0.576}Dy_{0.04})_2SiO_5$	$(Lu_{0.437}Gd_{0.534}Dy_{0.029})_2SiO_5$	40Lu-60Gd
$(Lu_{0.192}Gd_{0.768}Dy_{0.04})_2SiO_5$	$(Lu_{0.220}Gd_{0.740}Dy_{0.039})_2SiO_5$	20Lu-80Gd
$(Gd_{0.95}Dy_{0.05})_2SiO_5$	$(Gd_{0.951}Dy_{0.0495})_2SiO_5$	GSO

4. Results and Discussion

4.1. Crystal Structures. It was found that the $(Lu_{1-x}Gd_x)_2SiO_5$:Dy solid solution crystals exhibit the Lu_2SiO_5 type structure for all Gd^{3+} amounts inserted into the LSO structure. It means that even the crystal containing almost 80 at% of gadolinium and 20 at% of lutetium does not grow in the GSO ($P21/c$) but in LSO ($C2/c$) type structure. As was expected, substituting Lu^{3+} for Gd^{3+} in the LSO crystal brings about the modification of crystal growth temperature, unit cell parameters, unit cell volume, and the crystal density. The highest temperature of 2000 °C corresponding to the 80Lu-20Gd sample is slightly lower than the LSO melting point of 2050 °C. On the other hand, the melting temperature of the 20Lu-80Gd (1835 °C) is higher than that of the GSO crystal (1770 °C). Unit cell parameters of LGSO solid solution systems vary within the LSO type structure. The increase of the unit cell as well as unit volume is in proportion to the content of Gd^{3+} ions in crystal owing to the dissimilarity in the ionic radii of cations (Lu^{3+} = 0.86 Å, Gd^{3+} = 0.94 Å). The density of the samples gradually decreases from 7.4 g/cm^3 in LSO to a value of 6.6 g/cm^3 in (20Lu-80Gd), the value very close to the density of the GSO system. Structural data, determined for investigated LSO:Dy, GSO:Dy, and LGSO:Dy crystals, are gathered in Table 2. It should be emphasized here that all structural data relate to the crystalline hosts because small amounts of Dy^{3+} impurity are irrelevant for structural changes. Figure 2 presents lattice constants and volumes of unit cells (upper picture) as well as the X-ray densities and melting temperatures (lower picture) of the investigated crystals drawn versus the concentration of Gd^{3+} in the LSO structure. On the basis of presented data, we can assume that the phase transition from the LSO to GSO type structure in the mixed $(Lu_{1-x}Gd_x)_2SiO_5$ crystals should occur for $0.9 < x < 0.8$ since the $(Lu_{0.1}Gd_{0.9})_2SiO_5$:$Ce^{3+}$ crystal has the $P21/c$ space group of the GSO crystal.[8] Considerations of the LSO and GSO crystal structures in terms of [O5Re$_4$] and [SiO$_4$] tetrahedra (Figure 3) can catch structural dissimilarities that might explain the obtained results. In the GSO structure, the corner-linked [O5Gd$_4$] tetrahedra form a two-dimensional network parallel to the (100) plane. The [SiO$_4$] tetrahedra are located into the wide meshes of this net ensuring charge balance and connection to the parallel-running units.[1] In Lu_2SiO_5, the [O5Lu$_4$] tetrahedra do not form a two-dimensional network but chains and double [O$_2$−Lu$_6$] tetrahedra running along the a-axis. The infinite chains of edge-sharing [O5Lu$_4$] tetrahedra connect with [O$_2$−Lu$_6$] motifs by isolated [SiO$_4$] tetrahedra. Such arrangement results in less condensed overall packing

Table 2. Structural and Physical Characteristics of Single and Mixed Oxyorthosilicate Crystals

			unit cell parameters (Å)					density (g/cm^3)	
melt composition (%)	space group	T_{melt} (°C)	a	b	c	β (deg)	cell volume V (Å^3)	$d_{X\text{-}ray}$	d_{exp}
LSO	$C2/c$	2050	14.27088	6.64592	10.26085	122.190	823.583	7.37	7.38
80Lu-20Gd	$C2/c$	2000	14.30475	6.66549	10.31712	122.189	832.520	7.18	7.14
60Lu-40Gd	$C2/c$	1940	14.34939	6.69426	10.37889	122.175	843.875	6.98	6.98
40Lu-60Gd	$C2/c$	1890	14.41165	6.72676	10.44960	122.170	857.501	6.76	6.77
20Lu-80Gd	$C2/c$	1835	14.44016	6.74746	10.56265	122.121	871.630	6.55	6.62
GSO	$P21/c$	1770	9.13842	7.07454	6.85183	107.696	844.024	6.66	6.59

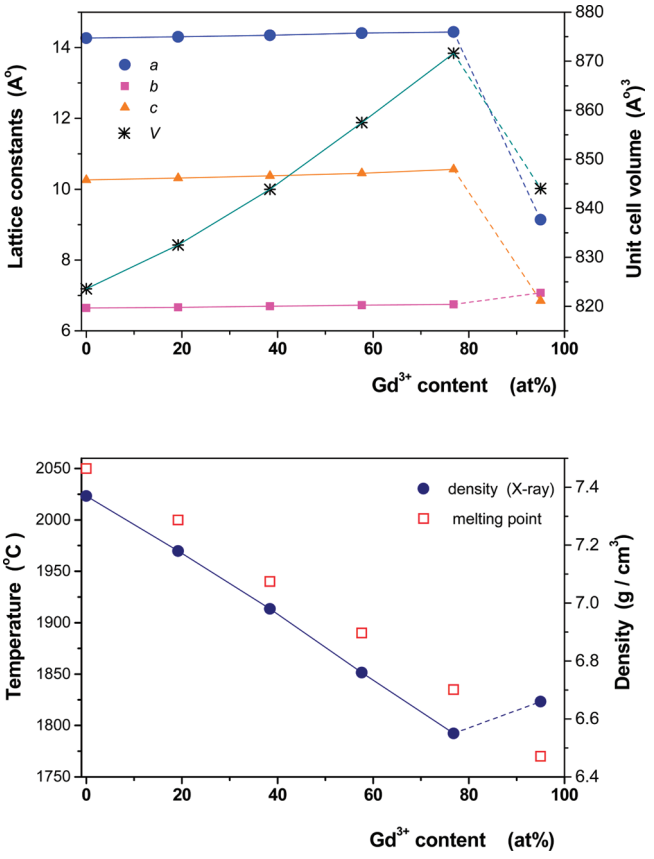

Figure 2. Variations of the structural (lattice constants, unit cell volume) (top panel) and physical (melt temperature, density) (bottom panel) parameters determined for the $(Lu_{1-x}Gd_x)_2SiO_5$ crystals with different concentrations of Gd^{3+} ions (x = 0, 0.2, 0.4, 0.6, 0.8, 1).

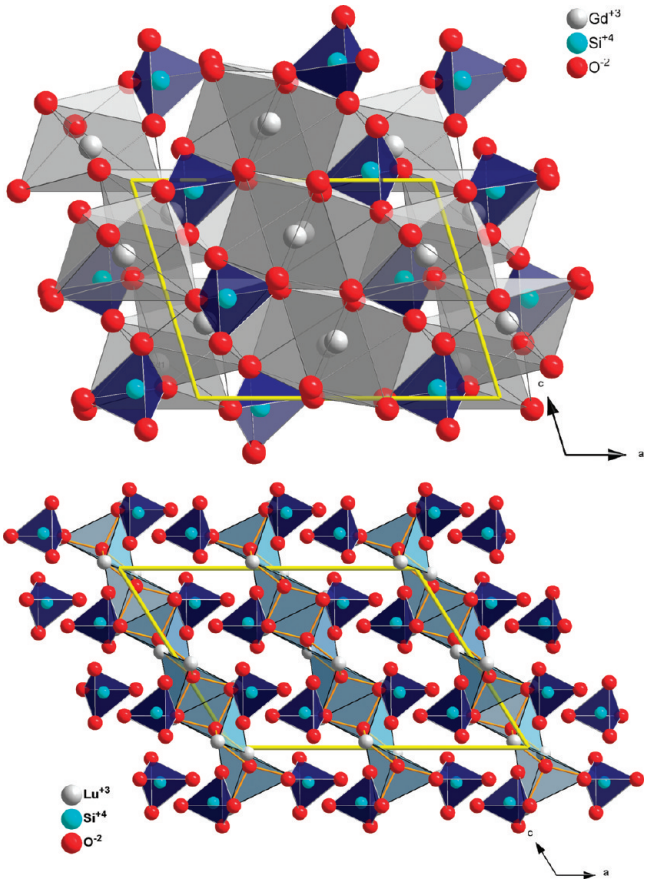

Figure 3. Views of the Gd_2SiO_5 (upper view) and Lu_2SiO_5 (lower view) crystals, illustrating the packing of the cationic polyhedra in unit cells.

in LSO than in GSO structure. We suppose that this feature protects the $C2/c$ structure of the $(Lu_{1-x}Gd_x)_2SiO_5$ crystals even for large amounts of Gd^{3+} ions ($x \leq 0.8$).

The attribution to a monoclinic system implies a biaxial character of the LSO and GSO crystals. Optical indicatrix axes D_1, Y, D_2 are not collinear with crystallographic a, b, c ones. Therefore, the LSO and GSO single crystals were oriented using a single crystal X-ray diffractometer (Xalibur Oxford Differential Company), and then, the position of optical axes in relation to crystallographic axes were determined examining conoscopic figures under a polarization microscope. Correlations between optical and crystallographic axes, not reported up to now, are presented in Table 3 together with characteristics of cationic sites and data reported for Y_2SiO_5[9] that is isostructural to LSO.

4.2. Optical Properties. It has been shown in our previous papers[5,6] that despite the optically biaxial character of the hosts, the anisotropy of optical spectra of Dy^{3+} in LSO and GSO crystals is rather weak. Therefore, in the present study, the absorption spectra were recorded with unpolarized light. Optical studies of the Dy^{3+}:LGSO crystals, carried out in the VUV−NIR spectral range, confirm structural results. Figure 4a,b presents low-temperature absorption spectra of the 80Lu-20Gd and 20Lu-80Gd attributed to transitions from the $^6H_{15/2}$ ground state to multiplets of the ^6H and ^6F terms of Dy^{3+}. In contrast to transitions in the UV−vis range, they are easy to interpret. The spectra are compared to those of LSO:Dy and GSO:Dy. The spectra are calibrated in units of absorption cross section (cm^2) to facilitate the assessment of absorption intensities. The bands of Dy^{3+} in the solid solution crystals exhibit a character of the LSO:Dy system even for the sample highly doped with Gd^{3+} ions. However, observed lines, quite broadened and with poorly resolved crystal-field structure, imply a considerable disorder in the structure of solid solutions in which small lutetium ions are replaced by large amounts of much bigger gadolinium. As an example, transitions to the $^6F_{3/2}$ and $^6F_{5/2}$ levels are shown in Figure 4b. Six well-resolved spectral lines of Dy^{3+} in two structural sites are observed for the $^6H_{15/2} \rightarrow {}^6F_{5/2}$ transitions in both the LSO and GSO hosts, but only three lines are observed for the $(Lu_{1-x}Gd_x)_2SiO_5$:Dy samples. Their spectral positions are consistent with the line positions of LSO:Dy confirming thereby a shared type structure. A width at half-maximum (fwhm) of the $^6H_{15/2}(0) \rightarrow {}^6F_{5/2}(0)$ transition at 801 nm rises from 2.18 cm^{-1} in LSO:Dy to 40 and 68 cm^{-1} in 80Lu-20Gd and 20Lu-80Gd, respectively, indicating a considerably degree of structural disorder provoked by the presence of Gd^{3+} ions in the structure. It should be noted also that the band at about 1266 nm, related mainly to the $^6H_{15/2} \rightarrow {}^6F_{11/2}$ hypersensitive transition (HS), dominates the infrared part of measured spectra as long as the structure of the studied systems is $C2/c$.

Generally, hypersensitive transitions are very sensitive to the host (ligand environments). Although all studied crystals have the same ligand anions, the intensity of HS transitions in LSO:Dy and LGSO:Dy solid solution crystals are roughly three times higher than that of GSO:Dy. It seems that a different symmetry of the LSO, LGSO ($C2/c$), and GSO ($P21/c$)

Table 3. Optical Axes and Site Characteristics of Lutetium, Gadolinium, and Yttrium Oxyorthosilicates

crystal	acronym	axis correlation	cationic sites	point symmetry	CN number[a]	ref
Lu_2SiO_5	LSO	(D_1, *a*) = 21.98° Y//b	Lu1	C_1	CN = 7	present work
		(D_2, *c*) = 10.24°	Lu2	C_1	CN = 6	
Gd_2SiO_5	GSO	(D_1, *a*) = 30.30° Y//b	Gd1	C_{3v}	CN = 9	present work
		(D_2, *c*) = 41.20°	Gd2	C_s	CN = 7	
Y_2SiO_5	YSO	(D_1, *a*) = 23.80° Y//b	Y1	C_1	CN = 7	9
		(D_2, *c*) = 11.35°	Y2	C_1	CN = 6	

[a] CN number − coordination number of cationic site.

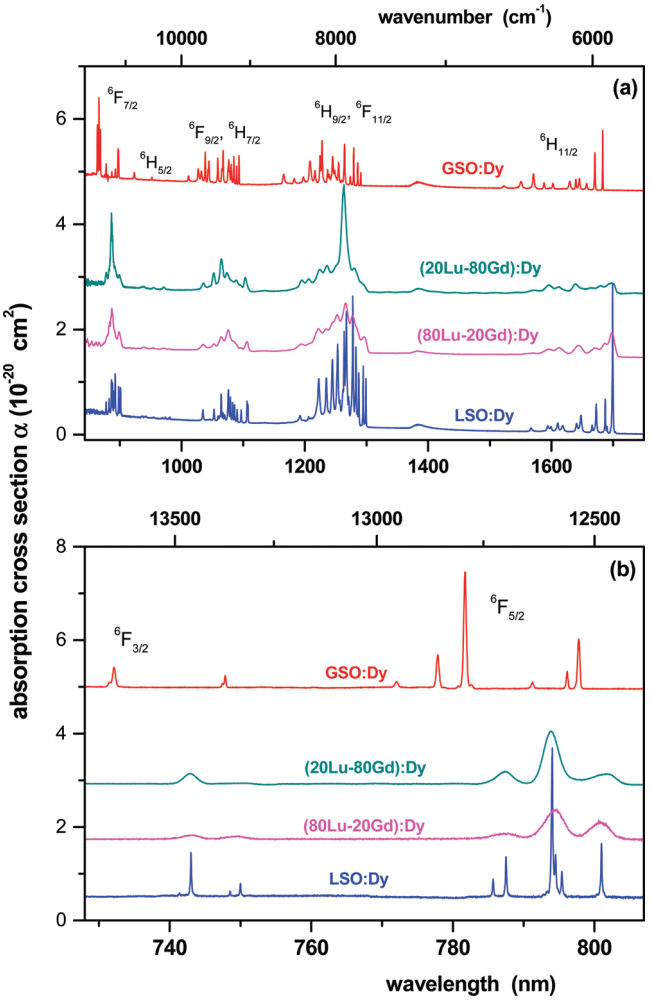

Figure 4. The comparison of absorption spectra recorded at 10 K in the near-infrared region for Dy^{3+}-doped systems under study.

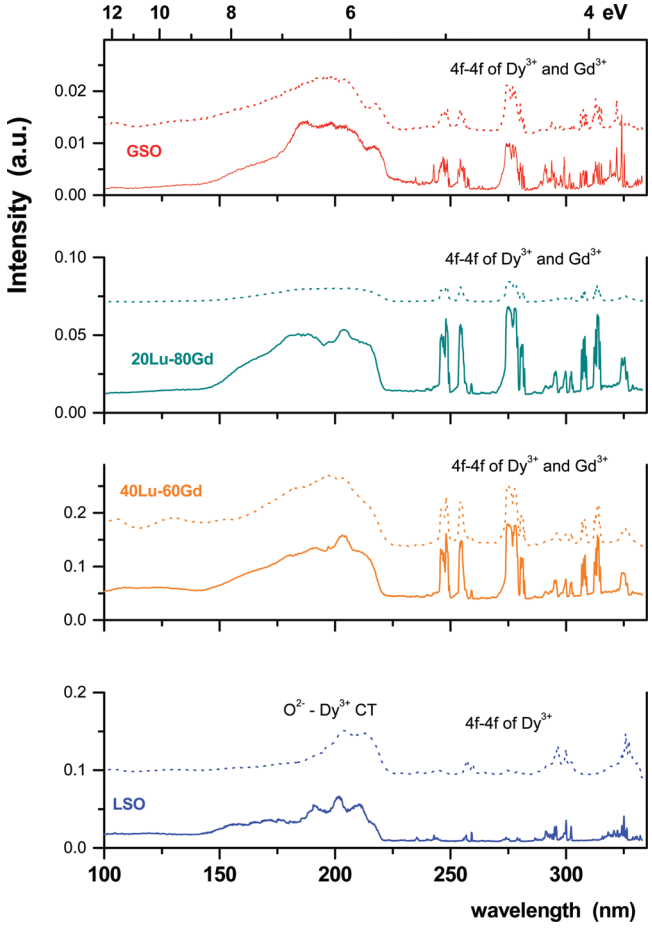

Figure 5. Excitation spectra of GSO:Dy, LGSO:Dy, and LSO:Dy crystals monitoring 576 nm emission ($^4F_{9/2} \rightarrow {}^6H_{13/2}$) from Dy^{3+} at 300 K (dotted spectra) and 12 K (solid spectra).

systems determines the intensity of transitions at around 1266 nm.

Monitoring the $^4F_{9/2} \rightarrow {}^6H_{13/2}$ emission of Dy^{3+} at 576 nm, the excitation spectra were measured at 12 and 300 K. The spectra, presented in Figure 5, were corrected for the incident flux of the excitation beam using the sodium salicylates as a standard. Broad bands spreading from 140 to 225 nm with maxima at around 200 nm can be related to the $O^{2-}-Dy^{3+}$ charge transfer CT transitions. The spectral range of these transitions is in accordance with those of the $YAl_3(BO_3)_4$:Dy crystal,[10] and Dy-doped LaF_3 and YF_3 hosts including oxygen traces.[11] Multiline structure superimposed on the CT bands, clearly observed in low-temperature spectra, can be attributed to the f-d interconfigurational transitions having much smaller spectral bandwidths than the CT-ones and widely overlapping f-f transitions in the VUV-UV region. Thus, the VUV-UV spectra of the LSO, GSO, and LGSO systems are difficult to analyze unambiguously. However, there is no doubt that sharp and well-defined lines in the 231−335 nm range correspond to electronic transitions within the $4f^9$ configuration of Dy^{3+} and the $4f^7$ configuration of Gd^{3+} ions. A detailed spectroscopic analysis of Dy^{3+} in the GSO and LSO hosts has been reported in our previous papers.[5,6] The presence of the gadolinium lines in excitation spectra of Dy^{3+} emission indicates an efficient energy transfer between ions. Spectral positions of observed bands are nearly the same for all studied crystals. However, a different VUV response was observed. In contrast to the LSO:Dy and GSO:Dy systems, the LGSO:Dy crystals exhibit comparable intensities of the f-f and CT bands. Such result suggests that an energy transfer from the host to Ln^{3+} emitting centers is more efficient in solid solutions than in the basic crystals. Different excitation wavelengths from the synchrotron radiation SR were used to study channels of host−ion and

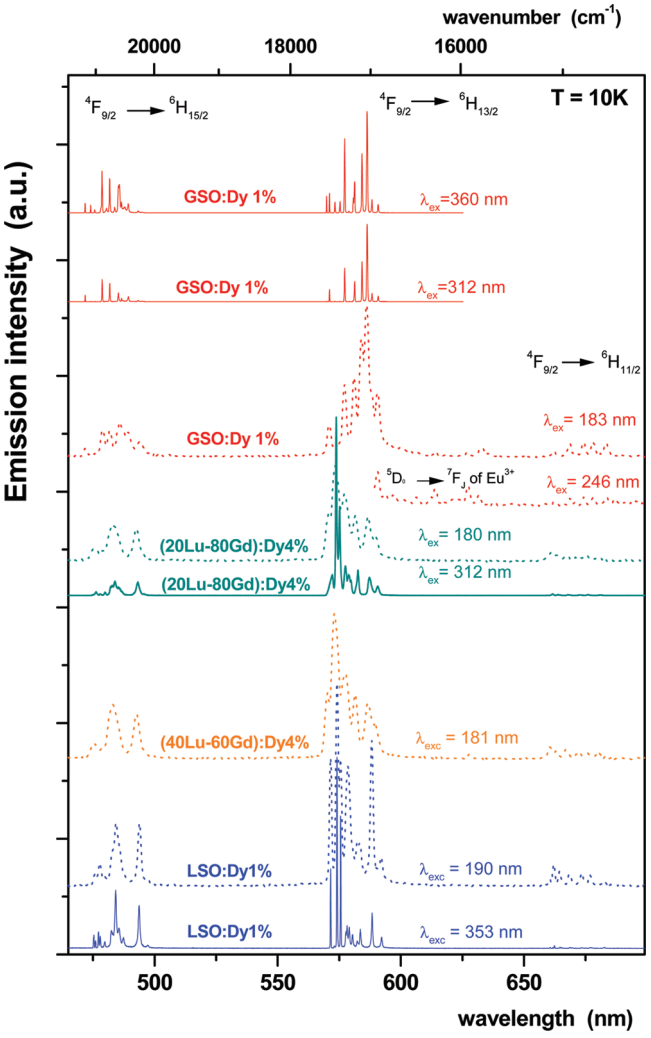

Figure 6. Low-temperature emission spectra excited by synchrotron radiation (dotted spectra) and by ozone-free Xe lamp (solid spectra).

ion−ion energy transfer processes contributing to the conversion of the VUV−UV excitation into the visible emission of Dy^{3+} ions and, maybe, the ultraviolet emission of Gd^{3+} ions. All the crystals were selectively excited at 12 and 300 K by wavelengths corresponding to the peaks of the 150−225 nm bands as well as by wavelengths related to gadolinium spectral lines at 246, 275, and 313 nm and dysprosium spectral line at 324 nm. Neglecting the line intensities resulting from the power of excitation beam, emission spectra of an individual crystal achieved by the 180−314 nm excitation wavelengths exhibit the same line structures. Hence, Figure 6 shows emission spectra of Dy^{3+} ions in the Lu_2SiO_5, Gd_2SiO_5, and $(Lu_{1-x}Gd_x)_2SiO_5$ ($x = 0.6$ and 0.8) hosts excited by 180 nm (dotted spectra) at 12 K. The observed lines are instrumentally broadened owing to a poor resolution of a CCD detector. However, they are consistent with high-resolution luminescence spectra (solid lines) measured at 10 K in the visible and near-infrared under the 312 and/or 360 nm excitation. Dysprosium luminescence, registered for all excitation wavelengths, is dominated by the visible emission in the yellow (575 nm) and blue (484 nm) that corresponds to the $^4F_{9/2} \rightarrow {}^6H_{13/2}$ and $^4F_{9/2} \rightarrow {}^6H_{15/2}$ transitions. Also, a weak band in the red was attributed to the dysprosium luminescence ($^4F_{9/2} \rightarrow {}^6H_{11/2}$). The ultraviolet emission of Gd^{3+} ions, related to the $^6P_{7/2} \rightarrow {}^8S_{7/2}$ transition, manifests as a sharp and weak spectral line at 314 nm (not shown in Figure 6). It is noteworthy that emissions spectra of the crystals containing Gd^{3+} ions exhibit an additional emission band in the red which was tentatively identified as the $^5D_0 \rightarrow {}^7F_2$ luminescence of Eu^{3+} ions being a trace element of the starting Gd_2O_3 oxide. The results obtained under the VUV excitations clearly show that transfer of excitation energy among the highest energetic states of Gd^{3+} and Dy^{3+} leads up to the population of the $^4F_{9/2}$ state and to emission in the blue, yellow, and near-infrared ranges. The presence of Gd^{3+} spectral lines in excitation spectra of Dy^{3+} emissions (Figure 5) and a weak emission of Gd^{3+} ions implies that an efficient energy transfer from Gd^{3+} to Dy^{3+} occurs. Moreover, the excited Gd^{3+} ions interact also with Eu^{3+} although its concentration is extremely low. Emission lines of the LGSO:Dy crystals exhibit more similarity to those of LSO:Dy than to GSO:Dy ones, regardless of the excitation wavelength. Such result indicates that, in contrast to the $Dy:Gd_2SiO_5$, neither of Dy^{3+} sites in $Dy:(Lu_{1-x}Gd_x)_2SiO_5$ is preferred by the $Gd^{3+} \rightarrow Dy^{3+}$ energy transfer, and Dy^{3+} ions in the LGSO matrix do not form isolated luminescence centers like in the Dy:LSO system. This feature can be distinctly seen in emission spectra presented in Figure 6.

A substantial broadening of dysprosium emission lines in LGSO confirms a structural disorder produced by the presence of much large Gd^{3+} ions in the ordered LSO structure. It is also reflected in the intensity parameters Ω_t and selected spectroscopic parameters (Figure 4) derived by the Judd-Ofelt standard method which was applied to the unpolarized absorption spectra.

4.3. Dynamics of the $^4F_{9/2}$ Luminescent State. To obtain additional information on luminescence properties of Dy^{3+} in the LGSO solid solution crystals, the dynamics of the $^4F_{9/2}$ emitting level was investigated at 10 and 300 K. The samples were resonantly excited into the $^4I_{15/2}$ level ($\lambda_{exc} = 454$ nm) with light pulses delivered by the OPO and the yellow and blue emissions were monitored. Temperature and the wavelength of monitored emission did not influence the character of decays and the lifetimes. Semilogarithmic plots of luminescence decays at 300 K under monitoring the yellow emission are shown in Figure 7. Presented curves, nonexponential in the initial stages of decays, turn afterward into exponential time-dependences (marked by solid lines) with time constants somewhat over 300 μs. The observed time-dependences are typical for a luminescence decay involving a self-quenching of emission via cross-relaxation process when the energy migration over donor ions does not occur. Focusing on the overall character of decays, the mean time constants, defined as

$$\tau_{mean} = \frac{\int_{t=0}^{\infty} tI(t)\,dt}{\int_{t=0}^{\infty} I(t)\,dt} \qquad (1)$$

where $I(t)$ is the intensity of luminescence at the time t, were estimated. Neglecting the minor differences in the Dy^{3+} concentrations, the experimental lifetimes of the $^4F_{9/2}$ level in the LGSO:Dy solid solutions and LSO:Dy crystal are nearly the same ($\tau_{mean} = \sim 263$ μs in LGSO:4%Dy, $\tau_{mean} = 202$ μs in LSO:5%Dy) and substantially longer than that in GSO:5%Dy ($\tau_{mean} = 118$ μs). Furthermore, taking into account the presence of two dysprosium sites in both LSO and GSO crystal structure, we can presume that the total relaxation rates of the $^4F_{9/2}$ state in the LGSO:Dy are the

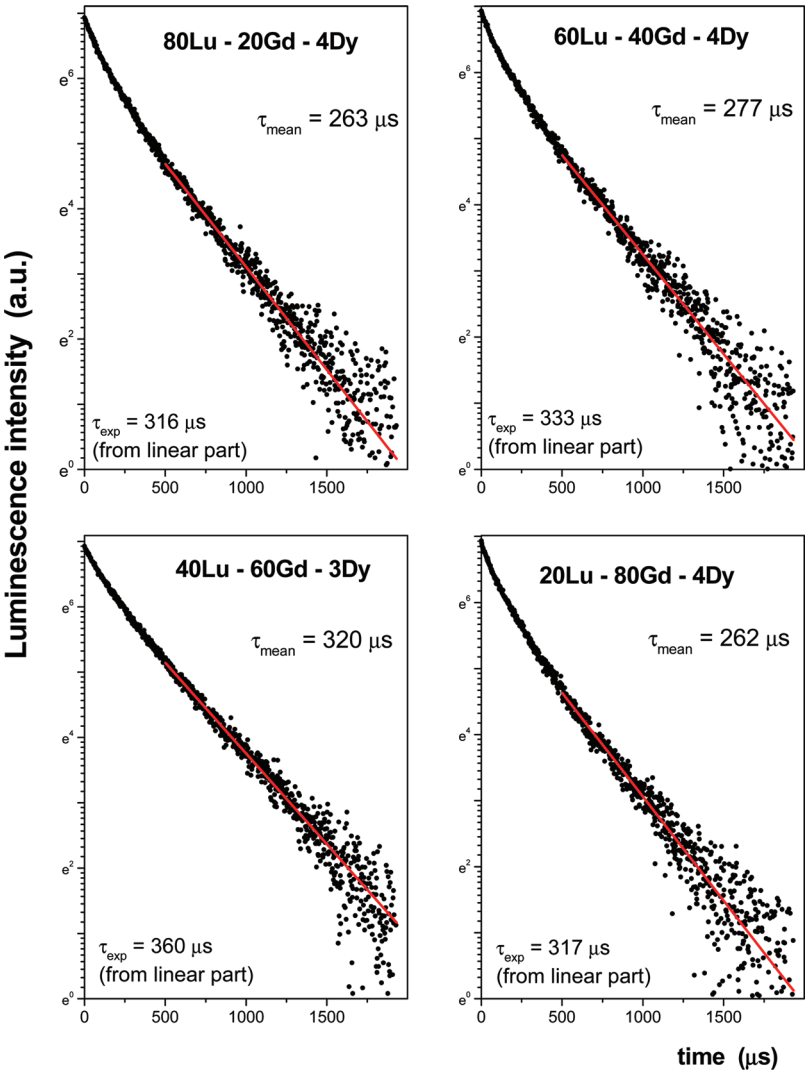

Figure 7. Emission decays of the $^4F_{9/2}$ level in $(Lu_{1-x}Gd_x)_2SiO_5$:Dy (x = 0.2, 0.4, 0.6, 0.8) recorded at 300 K under excitation into the $^4I_{15/2}$ state of Dy^{3+} and monitoring the 586 nm transition. Solid lines represent exponential parts of the decays.

same for both sites like in the LSO:Dy crystal[6] and unlike in GSO:Dy one.[5] The initial nonexponential stages of the recorded decays, arising from the static quenching with the Forster-like time dependence, and concentration variations of luminescence decays point out a significant role of nonradiative energy transfer by $Dy^{3+}-Dy^{3+}$ interactions. Nonradiative decays by multiphonon emission are expected to be negligibly small in all studied crystals owing to the large energy gap between the $^4F_{9/2}$ luminescent level and the lowerlaying $^6F_{1/2}$ level ($\Delta E \sim 7000$ cm^{-1}) as compared with energies of vibrational modes of Si−O bonds involved. Therefore, mainly an effective nonradiative energy transfer among Dy^{3+} ions influences the total relaxation rate of the $^4F_{9/2}$ state in the considered matrices. This process occurs via cross relaxation and is frequently observed in crystals containing a high concentration of dopant.

5. Dielectric Properties

Spectroscopic investigations reported above provide information on structural peculiarities on a microscopic scale, that is, in the near surrounding of dysprosium ions which can be regarded as probes of the crystal-field strength and symmetry in sites occupied by Gd^{3+} and Lu^{3+} ions. However, the crystal quality is governed mainly by the content of various kinds of macroscopic defects, among others bubbles, substructures, and inclusions which are difficult to determine based on spectroscopic data. Dielectric characteristics have been examined with the intention to get a closer insight into structural imperfections of solid solution crystals grown in this study.

The complex dielectric permittivity ε^* of the Dy-doped the Lu_2SiO_5, $(Lu_{1-x}Gd_x)_2SiO_5$, and Gd_2SiO_5 crystals, generally defined as

$$\varepsilon^* = \varepsilon' - i\varepsilon'' = \varepsilon_\infty + \frac{\Delta\varepsilon}{(1+(i\omega\tau)^\alpha)^\beta} + A(i\omega)^{s-1} + \frac{\sigma_{DC}}{i\omega\varepsilon_0} \quad (2)$$

was analyzed through the relaxation and conductivity processes represented by the Havriliak−Negami (H−N) relationship[12] and the Jonscher power law[13] with addition to the direct current (DC) conductivity σ_{DC}. The meaning of symbols is as follows: $\Delta\varepsilon$ is the dielectric strength, τ is the characteristic relaxation time of the process, α and β are the band shape parameters, the A is the real coefficient, and s is the Jonscher parameter describing the alternative current conductivity. The ε_0 and ε_∞ represent the permittivity of free space and high-frequency limit dielectric constant, respectively. The values of the real permittivity ε' together with the values of the

Table 4. Emission Transition Probabilities A_{rad}, Branching Ratios β, Radiative Lifetimes τ_{rad} and Intensity Parameters Ω_t of Dy^{3+} in LSO, LGSO, and GSO[a]

	crystal					
parameters	LSO	80Lu-20Gd	60Lu-40Gd	40Lu-60Gd	20Lu-80Gd	GSO
A_{rad} (s^{-1})[b]	1574	1544	1424	1378	1176	1845
β (%)						
$^4F_{9/2} \rightarrow {}^6H_{15/2}$	18	21	15	14	18	28
$^4F_{9/2} \rightarrow {}^6H_{13/2}$	68	61	69	70	68	54
τ_{rad} (μs)	635	648	702	726	850	542
Ω_t (10^{-20} cm^2)						
Ω_2	4.3136	4.3136	6.6410	6.6028	5.1124	3.2230
Ω_4	1.2759	1.2759	2.1040	2.1530	1.3739	2.1628
Ω_6	3.4939	3.4939	1.5638	1.3849	1.5929	3.7620

[a] Branching ratios for transitions to $^6H_{15/2}$ and $^6H_{13/2}$ are presented only. [b] $A_{rad} = \sum_j A_{rad}$, $\beta = A_{rad}/\sum_j A_{rad}$ and $\tau_{rad} = 1/\sum_j A_{rad}$.

Table 5. Selected Dielectric Parameters of the Dy-Doped Oxyorthosilicate Crystals[a]

crystal	σ_{DC} (10^{-8} S × cm^{-1})	$E_{\sigma(DC)}$ (eV)	ε'	E_τ (eV)	τ_m (s)
LSO-5Dy	1.70	1.18	14.8	1.31	4 (10^{-12})
80Lu-20Gd-4Dy	4.50	1.25	14.9	1.23	7 (10^{-12})
60Lu-40Gd-4Dy	0.47	1.35	15.3	1.26	5 (10^{-12})
40Lu-60Gd-3Dy	0.70	1.57	15.2	1.30	4 (10^{-12})
20Lu-80Gd-4Dy	0.60	1.81	15.1	1.24	2 (10^{-13})
GSO-5Dy	0.98	1.44	17.8	1.25	8 (10^{-10})

[a] σ_{DC} - conductivity at 1070 K. $E_{\sigma(DC)}$ - activation energy. ε' - real permittivity at 300 K. E_τ - activation energy of the relaxation process. τ_m - mean time of the dielectric relaxation.

DC conductivity σ_{DC}, activation energy and dielectric relaxation time constants, all derived from experimental data, are presented in Table 5. One can see that at room temperature the real permittivities ε' of the LGSO:Dy solid solutions are much alike and close to ε' of LSO:Dy even for large amounts of Gd^{3+} ions in the structure. The considered values, changing from 15.1 to 14.8 for 20Lu-80Gd and LSO, respectively, are lower than that of GSO:Dy amounting to 17.8. The complex dielectric permittivity versus temperature and frequency was studied. For the sake of the congruity of the obtained patterns and the clarity of graphic, Figure 8 presents only data acquired for the Gd_2SiO_5 sample. It is noteworthy that up to 573 K the permittivity ε' is constant (panel a), whereas the imaginary one slightly diminishes with the frequency (panel b). With the temperature increasing a visible step shifting toward higher frequencies characterizes the ε' curves. Such behavior might be related to some relaxation process. Above 773 K both components of permittivity increase with temperature by several orders and exponentially diminish with the frequency probably as a result of a conductivity process. The temperature dependence of σ_{DC} is presented in Figure 9. The presented data relate to the 700−1100 K temperature range because of a strong overlapping of the relaxation and conductivity processes at lower temperatures. The electric conductivity of the order of 10^{-13} (S × cm^{-1}) was found at 300 K indicating relatively good insulator properties of the crystals under study. However, a significant increase of the conductivity with temperature was observed, and at 1070 K the conductivity achieves values within a 0.47 (10^{-8} S × cm^{-1}) to 4.50 (10^{-8} S × cm^{-1}) range depending on the crystal composition (c. p. Table 5). The obtained dependencies can be described by the Arrhenius relation. Activation energies, estimated for thermally stimulated processes and presented in Table 5, increase from 1.25 to 1.81 eV with the growing concentration of Gd^{3+} in the $(Lu_{1-x}Gd_x)_2SiO_5$:Dy crystals and attain values higher than those of Lu_2SiO_5:Dy (1.18 eV) and Gd_2SiO_5:Dy (1.44 eV).

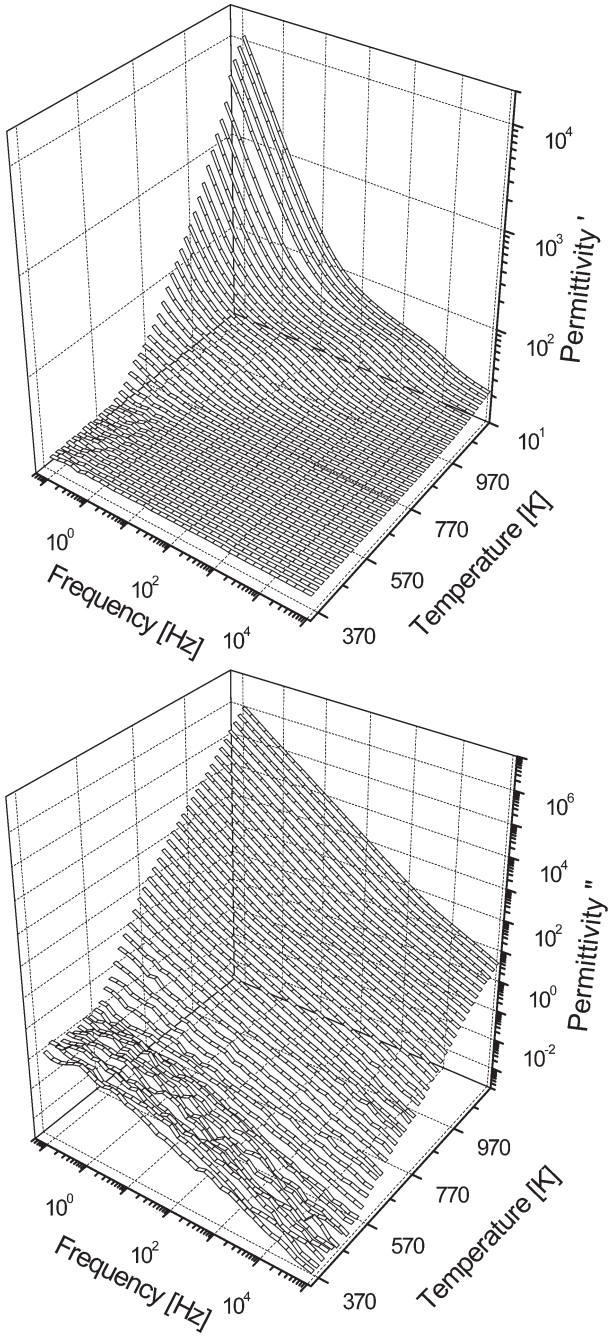

Figure 8. Frequency and temperature dependencies of real (top) and imaginary (bottom) parts of complex dielectric permittivity of the Gd_2SiO_5 crystal.

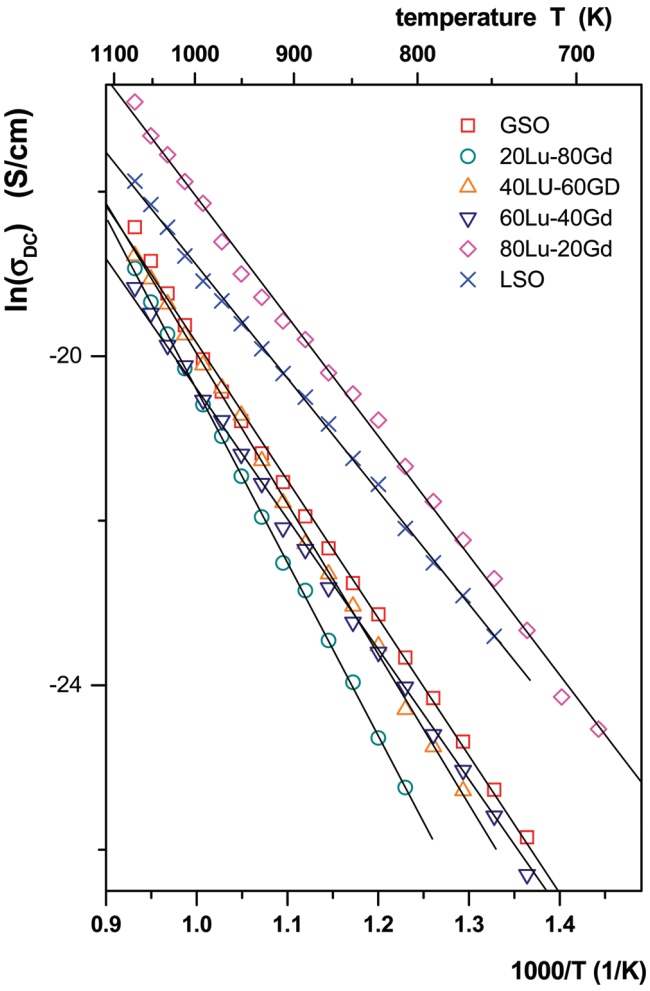

Figure 9. The DC conductivity versus temperature measured for the crystals under study. Solid lines represent the Arrhenius approximation.

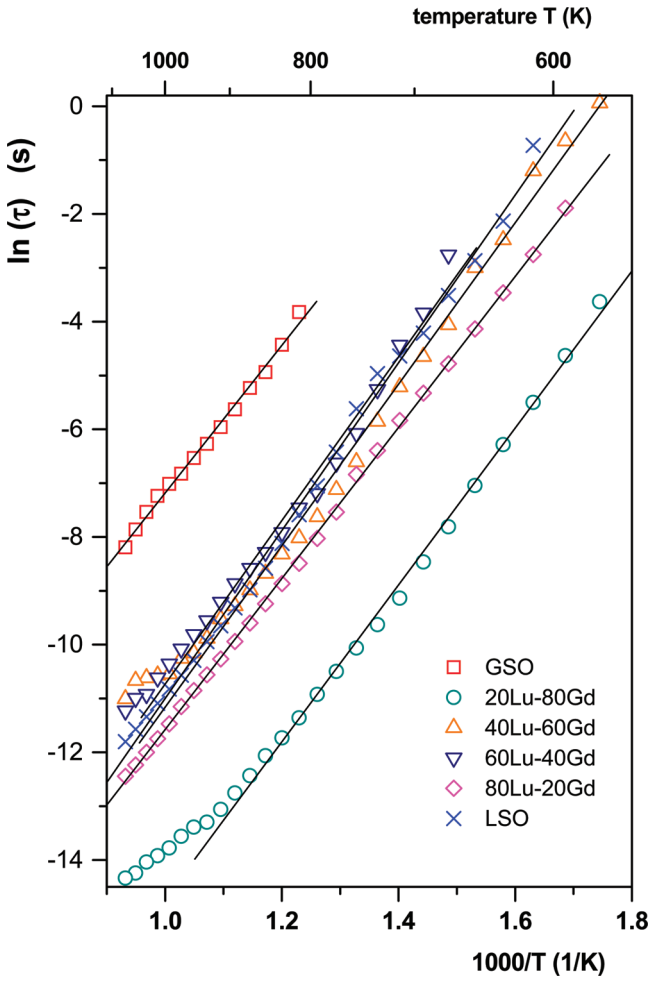

Figure 10. The temperature dependence of relaxation time measured for the LSO, LGSO, and GSO matrices doped with Dy^{3+} ions. Solid lines represent the Arrhenius approximation.

The studied crystals grow in an oxygen-free atmosphere and the creation of oxygen vacancies is highly probable during the process. Investigations of oxygen vacancies in LSO:Ce^{3+} by using the first-principles pseudopotential method disclosed that among five oxygen vacancy types (V_{O1}−V_{O5}) in the LSO matrix, the lowest formation energy of 1.75 eV is expected for non-silicon-bonded oxygen vacancies V_{O5} that are surrounded only by lutetium ions creating bonds with more ionic character than those of Si−O(1−4).[14] However, the most important factor influencing the crystal quality seems to be the devation from the crystal stoichiometry. At high temperature, the vaporization of the melt occurs. A higher rate of the SiO_2 vaporization as compared to that of the Lu_2O_3 vaporization[15] favors nonstoichiometric crystal composition and one may suppose that the importance of deviation from the stoichiometry will increase with an increasing melt temperature. In fact, the examination of experimental data in Figure 9 reveals that the LSO and 80Lu-20Gd crystals show distinctly higher conductivity than the remaining LGSO solid solutions and GSO crystals. On the basis of this result and crystallographic structures of investigated crystals, we can assume that observed conductivity is related to the ion and/or vacancy movement. The estimated values of Jonscher parameter ($s \leq 0.5$) suggest hopping rather than diffusion process in our systems which confirms the legitimacy of our assumption.

The influence of temperature on relaxation time constants of LSO, LGSO, and GSO hosts are presented in Figure 10. The relaxation process can be described by the activation energy E_τ and mean time constants τ_m. The band shape parameters α and β of 0.95 were estimated for LSO. The lower α values of 0.7, determined for the GSO and LGSO matrices, suggest the presence of the relaxation time distribution. The β parameters were close to unity, except the $(Lu_{0.2}Gd_{0.8})_2SiO_5$ host characterized by $\beta = 0.7$. The relaxation process observed in studied crystals may be related to macroscopic host defects. Both inclusions of Lu_2O_3 particles that were identified in the LSO matrix with scanning electron microscope SEM study[15] and/or the dislocation lines surrounded by charged defects should influence dielectric properties of a perfect host. It is reasonable to assume that charges created on the border spaces may be responsible for the Maxwell−Wagner type polarization effect. Structural data of the LGSO:Dy solid solution crystals, presented in this paper, imply that the phase transition from the Lu_2SiO_5 to Gd_2SiO_5 type structure is expected for Gd^{3+} concentration $x > 0.8$. Thus, we can suppose that, among all the solid solution samples, the $(Lu_{0.2}Gd_{0.8})_2SiO_5$:Dy crystal is the closest to a phase-transition composition and the breaking of the LSO type structure. Thus, some additional imperfection in this lattice can appear.

Presented results revealed that dielectric properties of the studied crystals are dominated by at least two overlapping

processes: the conductivity and relaxation processes. It was found that the movement of differently bonded charge carriers are responsible for observed dielectric properties. It seems that a dissimilarity in the Lu_2SiO_5 and Gd_2SiO_5 structures may be responsible for their different dielectric features. The increase of Gd^{3+} amount in the $(Lu_{1-x}Gd_x)_2SiO_5$ solid solution crystals brings about the reduction of the DC conductivity and the monotonous increase of activation energies. We assume that the origin of these changes comes from structural diversity of silicon-bonded and non-silicon bonded oxygens (and oxygen vacancies) in the LSO and GSO structures, the structural disorder observed in the LGSO crystals and the structural complexity in these materials.

6. Conclusions

The Dy^{3+}-doped $(Lu_{1-x}Gd_x)_2SiO_5$ solid solution single crystals with $x = 0.2, 0.4, 0.6$, and 0.8 were grown by the Czochralski method and their structural, physical, optical, and preliminary dielectric properties were investigated. It was found that their melting points are significantly lower than that of Lu_2SiO_5 crystal. Structural data reveal that the LGSO solid solutions belong to the LSO type structure even when the substitution of Lu^{3+} by Gd^{3+} in LSO amounts to 80%. On the basis of the variations of unit cell parameters, cell volume, melting temperature, and density versus composition, we suppose that the break of the LSO to GSO structure should occur for solid solution composition with $x > 0.8$.

The replacement of Lu^{3+} by Gd^{3+} leads to a structural disorder of the host manifesting in a substantial broadening of the spectral lines of optically active ions while influencing weakly the rates of their radiative and nonradiative transitions. The $(Lu_{1-x}Gd_x)_2SiO_5$:Dy solid solution crystals retain desirable luminescence and dielectric properties characteristic for $Dy:Lu_2SiO_5$ implying that they offer an interesting alternative to Lu_2SiO_5 host for optical applications. Evaluated dependence of the melting temperature on the chemical composition of the systems under study indicates that an important advantage of solid solution crystals over Lu_2SiO_5 crystal stems from the fact that they can be grown at lower temperature and hence more easily and cheaply.

Acknowledgment. The work was supported by Polish Ministry of Science and Information Society Technologies within a Grant No. N507 452034/2008-2010 and by IHP Contract No. II-05-096 EC of the European Commission. We would like to thank Prof A. Pietraszko from Institute of Low Temperature and Structure Research for the determination of optical axes and to Dr. M. Sobczyk from Faculty of Chemistry of Wrocław University for the ICP analysis.

References

(1) Felsche, J. *Struct. Bonding* (*Berlin*) **1973**, *13*, 99–197.
(2) Korzhik, M.; Fedorov, A.; Annenkov, A.; Borissevitch, A.; Dossovitski, A.; Missevitch, O.; Lecoq, P. *Nucl. Instrum. Methods Phys. Res. A* **2007**, *571*, 122–125.
(3) Moses, W. W. *Nucl. Instrum. Methods Phys. Res. A* **2002**, *487*, 123–128.
(4) Jacquemet, M.; Jacquemet, C.; Janel, N.; Druon, F.; Balembois, F.; Georges, P.; Petit, J.; Viana, B.; Vivien, D.; Ferrand, B. *Appl. Phys. B: Laser Opt.* **2005**, *80*, 171–176.
(5) Lisiecki, R.; Dominiak-Dzik, G.; Solarz, P.; Ryba-Romanowski, W.; Berkowski, M.; Głowacki, M. *Appl. Phys. B: Laser Opt.* **2010**, *98*, 337–346.
(6) Dominiak-Dzik, G.; Ryba-Romanowski, W.; Lisiecki, R.; Solarz, P.; Berkowski, M. *Appl. Phys. B: Laser Opt.* **2010**, *99*, 285–297.
(7) Young, R. A. *J. Appl. Crystallogr.* **1995**, *28*, 366–372.
(8) Loutts, G. B.; Zagumennyi, A. I.; Lavrishchev, S. V.; Zavartsev, Yu. D.; Studenikin, P. A. *J. Cryst. Growth* **1997**, *174*, 331–336.
(9) Li, C.; Wyon, C.; Moncorgé, R. *IEEE J. Quant. Elect.* **1992**, *1*, 1209–1221.
(10) Dominiak-Dzik, G.; Ryba-Romanowski, W.; Kovács., L.; Beregi, E. *Radiat. Meas.* **2004**, *38*, 557–561.
(11) Gérard, I.; Krupa, J. C.; Simoni, E.; Martin, P. *J. Alloys Comp.* **1994**, *207/208*, 120–127.
(12) Havriliak, S.; Negami, S. *J. Polymer. Sci. C* **1966**, *14*, 99–117.
(13) Jonscher, A. K. In *Dielectric Relaxation in Solids*; Chelsea Dielectric Press: London, 1983; p 83.
(14) Liu, B.; Qi, Z.; Gu, M.; Liu, X.; Huang, Sh.; Ni, Ch. *J. Phys.: Condens. Matter* **2007**, *19* (436215), 1–8.
(15) Ren, G.; Qin, L.; Li, H.; Lu, Sh. *Cryst. Res. Technol.* **2006**, *41*, 163–167.